JACS
JOURNAL OF THE AMERICAN CHEMICAL SOCIETY
Article
pubs.acs.org/JACS

Carboxylation and Decarboxylation of Active Site Lys 84 Controls the Activity of OXA-24 β-Lactamase of *Acinetobacter baumannii*: Raman Crystallographic and Solution Evidence

Tao Che,[†] Robert A. Bonomo,[‡,∥] Sivaprakash Shanmugam,[†] Christopher R. Bethel,[∥] Marianne Pusztai-Carey,[†] John D. Buynak,*[,§] and Paul R. Carey*[,†]

[†]Department of Biochemistry, and [‡]Departments of Medicine, Pharmacology, Molecular Biology and Microbiology, Case Western Reserve University, Cleveland, Ohio 44106, United States

[§]Department of Chemistry, Southern Methodist University, Dallas, Texas 75275, United States

[∥]Research Service, Louis Stokes Cleveland Veterans Affairs Medical Center, Cleveland, Ohio 44106, United States

Supporting Information

ABSTRACT: The class D β-lactamases are characterized by the presence of a carboxylated lysine in the active site that participates in catalysis. Found in *Acinetobacter baumannii*, OXA-24 is a class D carbapenem hydrolyzing enzyme that exhibits resistance to most available β-lactamase inhibitors. In this study, the reaction between a 6-alkylidiene penam sulfone inhibitor, SA-1-204, in single crystals of OXA-24 is followed by Raman microscopy. Details of its reaction with SA-1-204 provide insight into the enzyme's mode of action and help define the mechanism of inhibition. When the crystal is maintained in HEPES buffer, the reaction is fast, shorter than the time scale of the Raman experiment. However, when the crystal holding solution contains 28% PEG 2000, the reaction is slower and can be recorded by Raman microscopy in real time; the inhibitor's Raman bands quickly disappear, transient features are seen due to an early intermediate, and, at approximately 2−11 min, new bands appear that are assigned to the late intermediate species. At about 50 min, bands due to all intermediates are replaced by Raman signals of the unreacted inhibitor. The new population remains unchanged indicating (i) that the OXA-24 is no longer active and (ii) that the decarboxylation of Lys84 occurred during the first reaction cycle. Using absorbance spectroscopy, a one-cycle reaction could be carried out in aqueous solution producing inactive OXA-24 as assayed by the chromogenic substrate nitrocefin. However, activity could be restored by reacting aqueous OXA-24 with a large excess of $NaHCO_3$, which recarboxylates Lys84. In contrast, the addition of $NaHCO_3$ was not successful in reactivating OXA-24 in the crystalline state; this is ascribed to the inability to create a concentration of $NaHCO_3$ in large excess over the OXA-24 that is present in the crystal. The finding that inhibitor compounds can inactivate a class D enzyme by promoting decarboxylation of an active site lysine suggests a novel function that could be exploited in inhibitor design.

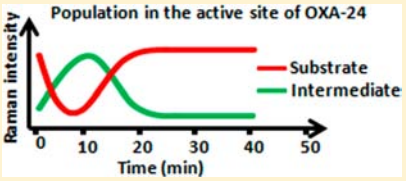

INTRODUCTION

Class D β-lactamases, also known as oxacillinases or OXA enzymes, due to their enhanced capability to hydrolyze oxacillin, can possess carbapenemase or extended-spectrum cephalosporinase activity[1−3] and are important determinants of antimicrobial resistance in Gram-negative pathogens, particularly including *Acinetobacter baumannii* and *Pseudomonas aeruginosa*.[4−7] Both *A. baumannii* and *P. aeruginosa* represent two of the most difficult pathogens to treat as they are often multidrug resistant (MDR) and pose a significant threat to hospitalized patients.[8] Class D enzymes are frequently not inhibited by the commercial β-lactamase inhibitors, clavulanic acid, sulbactam, and tazobactam. Unlike class A and C serine β-lactamases, the class D β-lactamases have a characteristic hydrolytic mechanism involving a carboxylated lysine residue, which is believed to function as the catalytic base, both during initial acylation of the active site serine and during hydrolysis of the intermediate acyl-enzyme, as shown in Scheme 1.[9,10] While there are examples of carboxylated lysine residues in other enzymes,[11,12] it is unusual for this residue to have a direct mechanistic role. One exception to this rule is the antibiotic sensor domain of the BlaR1 protein of the Gram-positive *Staphylococcus aureus*, which shares 28% sequence identity and high backbone homology with class D β-lactamases.[10,13] Rather than catalyzing the hydrolysis of penicillin like the class D β-lactamases, the BlaR1 sensor forms a stable acyl-enzyme with penicillins, leading to a conformational change in the protein; this relays a signal to the cytoplasm that derepresses the transcription of β-lactamase.[13−16]

The carboxylated lysine residue of the class D β-lactamases and the BlaR1 sensor are proposed to be crucial with respect to their differing behavior in the presence of β-lactams.[10,13] As noted by numerous investigators, the carboxy terminus of this residue is positioned analogously to E166 of the class A β-lactamases, and properly positioned to function as the catalytic base for both acylation and deacylation in class D β-lactamases. Lysine of the BlaR1 sensor undergoes decarboxylation subsequent to formation of the acyl-enzyme, thus removing the requisite

Received: April 2, 2012
Published: June 15, 2012

   dx.doi.org/10.1021/ja303168n | J. Am. Chem. Soc. 2012, 134, 11206−11215

Scheme 1. Reaction Pathway for Penicillin Hydrolyzed by OXA-24 β-Lactamase[19]

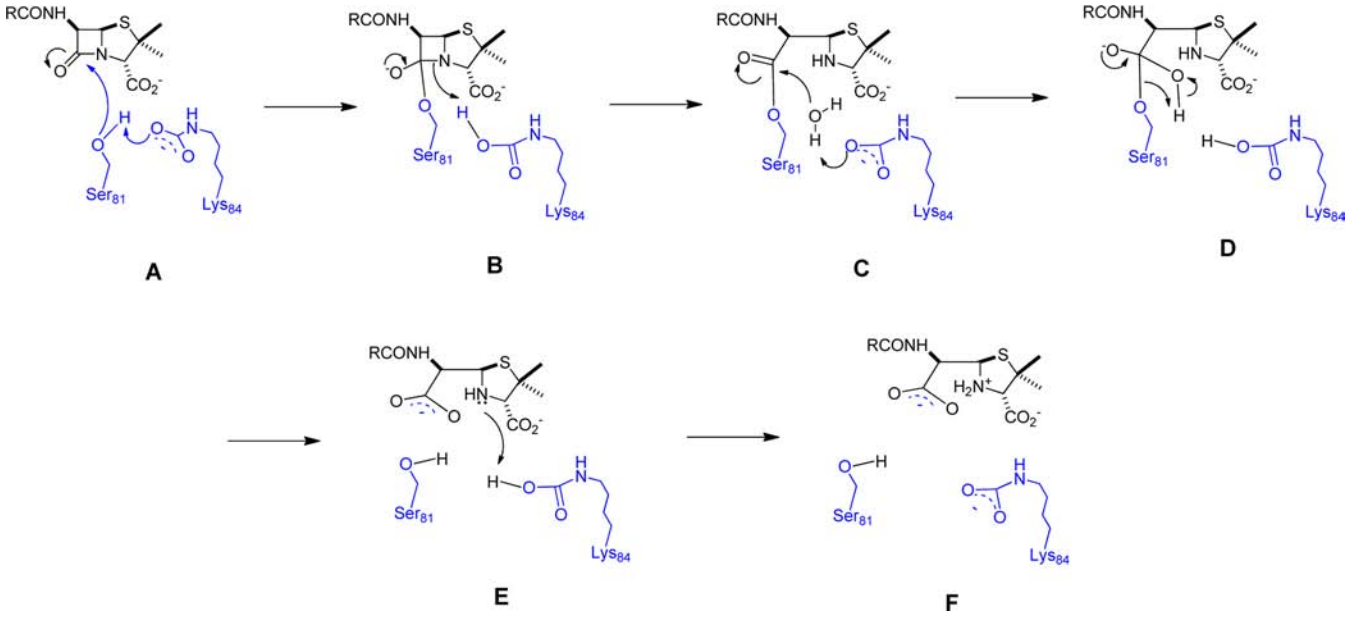

base from the vicinity of the acylated serine, and leading to a stable acyl-enzyme,[13,15] while in some cases the β-lactamases are able to retain the carboxy group and complete the hydrolytic cycle.

Structural and mechanistic features that promote the formation and stabilization of carboxylysine residues are poorly understood. Therefore, discerning the factors that allow class D β-lactamases to form and maintain a carboxylated lysine, while promoting decarboxylation of the analogous residue in BlaR1, could provide insight leading to design of more effective β-lactamase inhibitors.

To understand its chemical properties and potential decarboxylation pathways, a carboxylated lysine can be compared to the hypothetical carbamic acid (H_2NCO_2H). Carbamic acid is predicted to have a pK_a of 5.89 (COOH) and −1.22 (protonation of the nitrogen) (calculated using Advanced Chemistry Development (ACD/Laboratories) Software V11.02 (1994−2012 ACD/Laboratories), thus verifying the protonation occurs on the oxygen of the more basic, and properly positioned, carboxylate anion, and posing the mechanistic issue of how subsequent decarboxylation (and consequent transfer of the proton from oxygen to nitrogen) may occur. Calculations on the decarboxylation of the carbamic acid molecule indicate that the activation energy can be lowered by 44 kcal/mol by the assistance of one water molecule, as shown in Scheme 2.[17,18] Direct transfer of the proton from the (carboxy group) oxygen to the nitrogen, with appropriate geometry for the proton to interact with the nitrogen electron pair, while simultaneously maintaining the amide bond resonance, would involve a four-membered transition state and proton transfer over a distance of approximately 2.72 Å, as shown in Scheme 2A. The N−HO distance is reduced to 2.29 Å by rotating about the amide CO−N bond to the high energy conformation (Scheme 2B). By contrast, incorporating assistance from a neighboring water molecule, which could simultaneously provide H-bond donor and acceptor interactions with the carboxylated lysine, would involve a six-membered transition state and achieves optimal bond distances from the low energy amide conformation as shown in Scheme 2C. Bou et al.[19] recently proposed that the reason for the divergent behavior of class D β-lactamases and BlaR1 is the presence of a suitable water molecule to facilitate loss of CO_2 in BlaR1[20] and the absence of a corresponding water in the case of the β-lactamases, a difference potentially caused by the positioning of a highly conserved[1] hydrophobic valine (or isoleucine) residue at the β-lactamase position 130 (DBL consensus numbering) and a hydrophilic asparagine residue at corresponding position 109 in BlaR1 as illustrated in Figure 1.[21]

In this Article, we use Raman spectroscopy to explore the details of the reaction of OXA-24[2] with a 6-alkylidiene penam

Scheme 2. Addition of One Water Molecule Lowers the Activation Energy during the Decarboxylation Process of Carbamic Acid

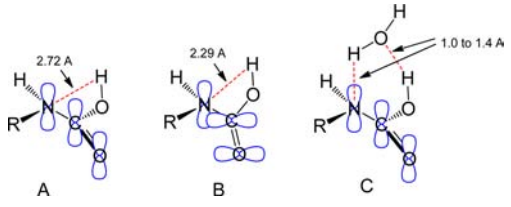

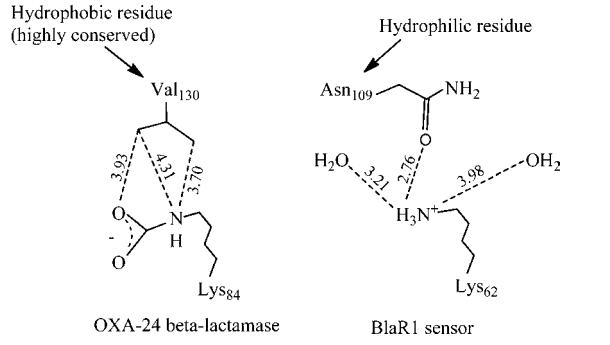

Figure 1. Comparison of the active-site carboxylysine environment of OXA-24 β-lactamase (PDB entry 3G4P) with BlaR1 sensor (PDB entry 1XA1).

dx.doi.org/10.1021/ja303168n | J. Am. Chem. Soc. 2012, 134, 11206−11215

sulfone inhibitor, SA-1-204 (Chart 1). This analysis provides novel insight into the enzyme's mode of action and shows that

Chart 1. 2′ β-(Phenylacetoxy)-6Z-(α′-pyridylmethylidene) Penicillin Sulfone, SA-1-204

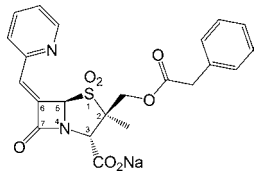

(de)carboxylation of Lys84 acts as a catalytic switch.[13] Earlier work concluded the reaction between SA-1-204 and OXA-1 or SHV-1 (a class A β-lactamase) in a single crystal occurs slowly in HEPES buffer, forming a noncovalent Michaelis-like complex that is stable in the active site up to 1 h before hydrolysis.[22] However, new evidence we obtained for SHV-1 (Shanmugam and Carey, unpublished work) shows that the reaction is actually fast in HEPES buffer and is complete in less than 3 min. For SHV-1, the reaction can be slowed by the addition of PEG 6000, which allows us to record the reaction including intermediate species using Raman microscopy, which is also the case as shown here for OXA-24. It is likely that the reaction is also fast in OXA-1 in the absence of PEG, but slow in the presence.

MATERIALS AND METHODS

Inhibitors. SA-1-204 was synthesized as described previously.[23] A stock solution of the inhibitor at 20 mM in 10 mM HEPES buffer (pH 7.5) was prepared for "soak in" experiments with the protein crystals and for UV−absorbance studies. Potency was verified using the colorimetric β-lactamase substrate nitrocefin (Becton Dickson, λ_{max} = 482 nm; ε = 17 400 M^{-1} cm^{-1}) .

Protein Isolation, Purification, and Crystallization. *E. coli* BL21 (DE3) cells including pET24 (+) plasmid vector containing bla_{OXA-24} have been described previously.[19] These cells were grown in super optimal broth (SOB) containing 50 μg/mL kanamycin at 37 °C in shaker flasks to achieve an OD_{600} around 0.6−0.8. Next, IPTG (isopropyl β-D-1-thiogalactopyranoside) was added to the culture with a final concentration of 0.2 mM, and the culture was grown for three more hours. The cells were spun down by centrifugation and frozen at −20 °C. The cultures were warmed back to room temperature and lysed by adding lysozyme and sonicating. The supernatant was collected for further purification. OXA-24 β-lactamase was purified by combination of gel filtration and ion exchange chromatography. A gel filtration HPLC (high pressure liquid chromatography) purification step was performed using a Sephadex Hi Load 26/60 column (GE Healthcare) and elution with 50 mM sodium phosphate buffer (pH 7.4). Ion exchange chromatography was performed using Q sepharose and elution with a NH_4HCO_3 gradient. Concentration of the protein was measured by Bio-Rad's protein assay, and the purity of the enzyme was evaluated by SDS-PAGE. Following purification, the OXA-24 β-lactamases were crystallized using the protocol of Bou et al.[19] Briefly, OXA-24 was concentrated to 6 mg/mL in 10 mM HEPES buffer (pH 7.5). Crystals were grown by the hanging drop vapor diffusion method in a crystallization solution containing 0.1 M HEPES (pH 7.5), 0.1 M sodium acetate, and 28% PEG 2000. The crystals were obtained in 4−6 days with the dimensions of 0.12 × 0.12 × 0.08 mm.

Raman Crystallography. The Raman microscope system has been described previously.[24,25] A single OXA-24 crystal was transferred from the mother liquor solution to a 4 μL drop of 0.1 M HEPES (pH 7.5), 0.1 M NaOAc, and 28% PEG 2000. A 647 nm, 80 mW Kr^+ laser beam (Innova 70 C, Coherent, Palo Alto, CA) was focused on the protein crystals in the 4 μL hanging drop using the 20× objective of the Raman microscope. During data collection, spectra were acquired for 10 s, and 10 accumulations were averaged for each time point. The spectrum of inhibitor SA-1-204 was first taken in the absence or presence of PEG. After spectra of the apo OXA-24 protein crystals were obtained, inhibitors were soaked into the drop to achieve a final volume of 5 μL and a final inhibitor concentration of 5 mM. Spectra were then acquired every 2−3 min after addition of the inhibitors. To obtain difference spectra, an apo β-lactamase spectrum was subtracted from the protein-inhibitor spectra at varying time intervals following addition of inhibitor (Supporting Information Text 1).

$$\text{Raman difference spectrum} = [\text{protein} + \text{inhibitor}] - [\text{protein}]$$

Absorbance Studies. For the $NaHCO_3$ reactivating experiment in a 500 μL reaction system with or without 28% PEG, OXA-24 was mixed with SA-1-204 in the presence or absence of $NaHCO_3$. Nitrocefin was used as a chromogenic substrate for OXA-24. The final concentrations were OXA-24 5 μM, SA-1-204 50 μM, nitrocefin 20 μM, $NaHCO_3$ 100 μM or 100 mM. UV−visible absorbance spectra were taken. Each spectrum included absorbance at wavelengths (λ) from 200 to 600 nm. These spectra were recorded at 30 s intervals, with the length of the experiment 30 min. The spectra were saved as individual files grouped by experiment, and the spectra shown in Figure 4 are the average of these.

Calculations. Ab initio quantum mechanical calculations were performed on CWRU's cluster facility to predict the Raman spectra of SA-1-204 and model intermediate compounds using Gaussian 03.[26] Calculations were performed at the DFT5 level using the 6-31+G(d) basis set. DFT calculations were performed with Becke's three-parameter hybrid method using the correlation functional of Lee, Yang, and Parr (B3LYP). The vibrations giving rise to the most intense calculated peaks could be visualized using "GaussView", revealing which molecular vibrations contribute to the peaks.

RESULTS AND DISCUSSION

a. The Presence of PEG Can Decelerate the OXA-24 β-Lactamase Reaction with SA-1-204 Inhibitor. Previous studies in our lab indicated that the reaction between SA-1-204 (Chart 1) and OXA-1 in single crystal is slow, with little change occurring in the spectrum of the bound ligand in one hour.[22] However, crystallographic studies of several other 6-alkylidene-2′-substituted sulfones, with structures similar to the SA-1-204, reacting with OXA-24 in single crystals show that a quasi-stable bicyclic aromatic late intermediate (Z in Scheme 3) forms after 6 min soaks in the presence of PEG 2000.[19]

To compare the reaction in the presence or absence of PEG, we use Raman microscopy to study the reaction in single crystals in real time. At first sight, the data in Figure 2A, the time dependence of SA-1-204 reacting in an OXA-24 crystal in HEPES-based holding solution, suggest that no reaction has occurred from 2 to 50 min. However, close examination shows that weak peaks occur at 2 min like 1440 and 1322 cm^{-1} and then decrease with time. These peaks are assigned to late intermediate species Z in Scheme 3 in section 3.b. Essentially, these data suggest that one reaction cycle is complete at 2 min (the experimental "dead time" of our Raman approach) leaving a trace of late intermediate that is slowly hydrolyzed with time. At 2 min, most active sites are reoccupied by new SA-1-204, but this second molecule of substrate does not react because, as elucidated below, the active site is no longer functional. However, the situation is dramatically different when PEG is added to the holding solution. Figure 2B shows the time-dependent Raman difference spectrum for the inhibitor SA-1-204 reacting in single crystals of OXA-24 in mother liquor containing 28% PEG 2000. The results show that the reaction now occurs more slowly (Figure 2B). In the figure, at 2 min, the substrate peaks have almost disappeared and new peaks appear. In the presence of PEG, we can see not only the late

Scheme 3. Proposed Mechanism of OXA-24 β-Lactamase Inhibition by SA-1-204[a]

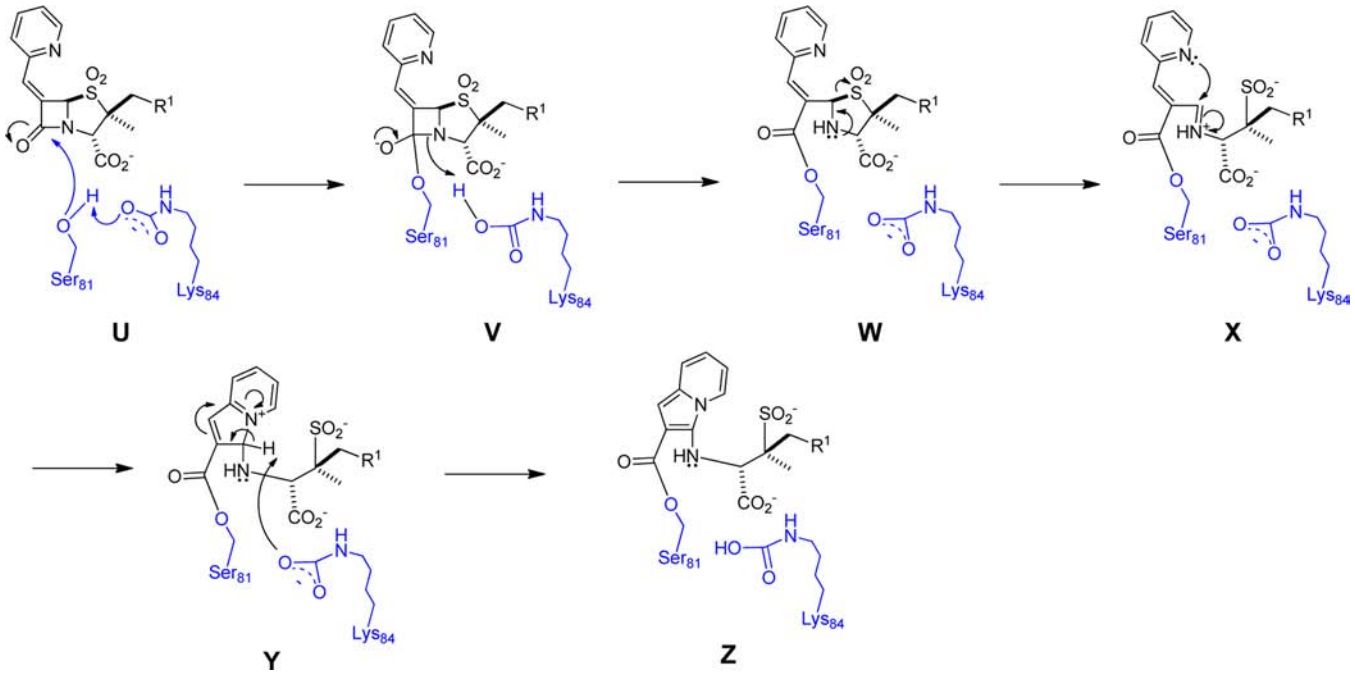

[a]In SA-1-204, R^1 is $-O(C{=}O)CH_2Ph$ (modified from Bou et al., 2010).[19]

intermediate peaks like 1443, 1339, and 1322 cm^{-1} (assigned below) but also peaks like 1657 cm^{-1} that decay rapidly and are assigned to an early intermediate X in Scheme 3 (section 3.b). This indicates that, at 2 min, the reaction is still proceeding, whereas we saw, in the absence of PEG, that the first cycle of the reaction was complete at 2 min.

The findings for the reaction in single crystals above also find support from the experiment undertaken in solution. We used nitrocefin to monitor the enzyme activity in solution in the presence or absence of PEG 2000 because nitrocefin produces an intense red chromophore in the presence of active β-lactamase. After 50 μM SA-1-204 was incubated with 5 μM OXA-24 in the absence of PEG, the enzyme activity was tested every minute. The result showed that the enzyme was completely inhibited at 1 min because the nitrocefin was not hydrolyzed and the red chromphore did not appear.[27] However, in the presence of PEG, the enzyme was still reactive after 5 min because nitrocefin was hydrolyzed and product was formed.[27] The enzyme was not completely inhibited until 10 min in the presence of PEG because acylation is slowed and active OXA-24 is present until about 10 min. In toto, the results indicate that in crystallo or in solution reaction is occurring quickly in HEPES-based solutions but is slowed markedly in solutions containing PEG.

Possible explanations for why 20−30% PEG can decrease the reaction velocity is that PEG may either slow the molecular diffusivity or necessary conformational changes in the active site due to increasing the viscosity of the solution. The viscosity generally increases when the concentration or the average weight of PEG increases.[28] Earlier work showed that PEG acts as a macroviscogen that can help increase the macroscopic viscosity of solution without slowing the rate of diffusion of small molecules in the solution.[29] Thus, in our experiment, the viscosity (η) of solution in the presence of 28% PEG 2000 in crystallo is estimated to be about 9.781 mPas, which is 9 times the viscosity of water (η = 1.0045 mPas).[28] The increase in viscosity of the solution due to the presence of PEG decelerates the reaction by slowing the conformational changes needed in the active site to form intermediates and products. The slower reaction in the presence of PEG allows us to visualize the progression of the reaction in crystallo in real time by use of Raman microscopy.

b. Reaction of SA-1-204 in OXA-24 Crystals Undergoes Only One Cycle. In the previous section, we propose that SA-1-204 reacts much faster in OXA-24 crystals surrounded by holding solution that does not contain PEG 2000. Under both sets of conditions with or without PEG, the OXA-24/SA-1-204 reaction goes through just one cycle resembling the reaction in Scheme 3. We now provide evidence to support this claim. First, we examine the kinetic data for the peaks occurring in the slower reaction in the presence of PEG (Figure 2B). This helps us assign the nonsubstrate peaks in Figure 2B to special features from postulated intermediate seen in Scheme 3. In turn, this allows us to identify peaks in the fast and slow reactions (Figure 2A and B) and show that it is likely that only one reaction cycle has occurred.

In the reaction of SA-1-204 in OXA-24 single crystal in the presence of 28% PEG 2000, the results show that the reaction occurs relatively slowly and appears to go through only one cycle (Figure 2B). In the figure, at 2 min, the substrate peaks have almost disappeared and new peaks appear. The peak at 1695 cm^{-1} in the spectrum is assigned to the methylenic double bond stretch coupled to the pyridine mode, which is expected to change markedly when the β-lactam ring opens and the hybridization at C6 changes (see below). Another characteristic feature is at 1761 cm^{-1}, which originates from the carbonyl (C=O) group of the intact lactam ring (see below). In previous reports of reactions between β-lactamases and inhibitors sulbactam, tazobactam, and clavulanic acid, the disappearance of this peak is ascribed to opening of the lactam ring and acylation of the enzyme.[30] In the present experiment, the peaks at 1761 and 1695 cm^{-1} disappear, showing that the reaction is occurring. The peak at 1000 cm^{-1} corresponds to the phenyl ring mode in SA-1-204 structure, which acts as an "internal standard" to monitor the

dx.doi.org/10.1021/ja303168n | J. Am. Chem. Soc. 2012, 134, 11206−11215

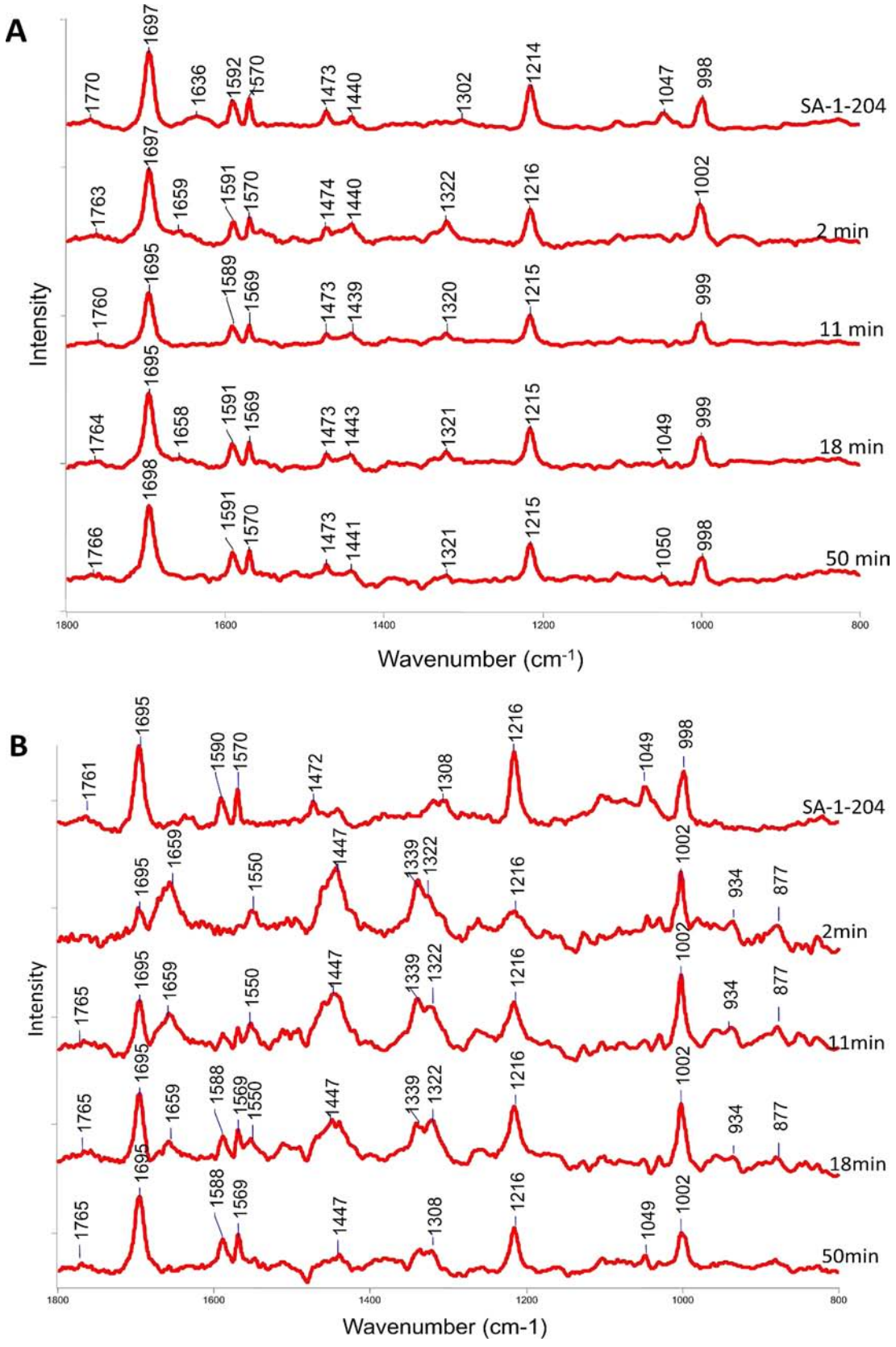

Figure 2. Raman difference spectra of OXA-24 single crystal reaction with SA-1-204 in the absence or presence of PEG 2000. (A) Raman difference spectrum of OXA-24 and SA-1-204 at 2, 11, 18, and 50 min in the absence of PEG. Control spectrum of unreacted SA-1-204 was first taken in the absence of PEG. After SA-1-204 was soaked in, the spectra were taken at the above indicated time points. The reaction is almost complete at 2 min. (B) Raman difference spectrum of OXA-24 and SA-1-204 at 2, 11, 18, and 50 min in the presence of PEG. Control spectrum of SA-1-204 was first recorded in the presence of PEG. After SA-1-204 was soaked in, the spectra were taken at the above indicated time points. The presence of PEG decelerates the OXA-24 β-lactamase reaction with SA-1-204 inhibitor.

dx.doi.org/10.1021/ja303168n | J. Am. Chem. Soc. 2012, 134, 11206−11215

reaction because it remains unchanged during the reaction (see below). At about 11 min (Figure 2B), the substrate peak at 1695 cm^{-1} begins to regain intensity probably as a result of product leaving the active site and the substrate reentering. After 11 min, the substrate peaks continue to "grow in" reaching a maximum at 50 min. Surprisingly, the substrate remains in the active site unchanged and does not appear to undergo catalysis.

On the basis of the structures of substrates similar to SA-1-204 and the constitution of the active site in OXA-24, the mechanism proposed by Bou et al.[19] is taken as a working model as shown in Scheme 3. To identify whether the proposed mechanism is consistent with the observed Raman spectra, ab initio quantum mechanical calculations were used to predict the Raman spectra for some of the species seen in Scheme 3. Using the Gaussian program,[26] calculations were performed for the free substrate, the early intermediate X, and the late intermediate Z (Scheme 3) because X-ray crystallographic data support their existence. For free substrate SA-1-204 (Table 1), the peaks at 1761 and 1695 cm^{-1} (Figure 2B) have

Table 1. Peak Assignment for Unreacted SA-1-204 from Gaussian Calculations

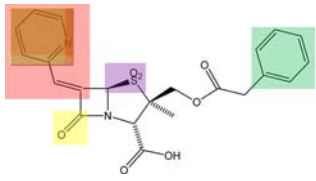

Calculation results of **unreacted SA-1-204**			
Experimental group (cm^{-1})	Calculated group (cm^{-1})	Raman intensity (calculated)	Peak assignment
1760	1745	128	
1695	1694	2335	
1588	1625	150	
1570	1625	88	
1472	1458	173	
1216	1252	197	
1000	998	30	

been described above (yellow and red regions, respectively, in the cartoon), as well as the peak at 1000 cm^{-1} (green region). On the basis of the Gaussian calculations, the other narrow features at 1588 and 1570 cm^{-1} (Figure 2A and B) have contributions from the $-SO_2-$ group and pyridine group motions (purple and orange regions, respectively, in the cartoon). The 1472 cm^{-1} feature is due to a pyridine mode (orange region), while the 1216 cm^{-1} mode is from methylenic stretch coupled to the pyridine modes (red region).

For the proposed intermediate X (Scheme 3 and Table 2), the intense peak at 1658 cm^{-1} (Figure 2B) is assigned to an in-plane mode involving pyridine and the skeleton to N4 (red region). The 1447 cm^{-1} peak derives from the ester group covalently linked to the enzyme (blue region). There are two intense vibrations predicted by the calculation that may be unresolved in the experimental 1658 cm^{-1} feature (Figure 2B). Amide I features from α-helices also appear near 1658 cm^{-1}.[31] However, it is unlikely that the 1658 band is due to changes in α-helices. These invariably give rise to a feature near

Table 2. Peak Assignment for Proposed Early Intermediate X from Gaussian Calculations

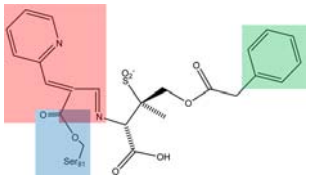

Calculation results of **early intermediate X**			
Experimental group (cm^{-1})	Calculated group (cm^{-1})	Raman intensity (calculated)	Peak assignment
1658	1658	859	
	1640	271	
1447	1458	103	
1000	998	42	

945 cm^{-1},[32−34] and there is no evidence for a time -dependent feature near 945 cm^{-1} in Figure 2. In addition, the assignment of the 1658 cm^{-1} to the protonated imine of intermediate X is further supported by calculations in the imine species in SHV-1 β-lactamase intermediates; this has a calculated and experimental band at 1658 cm^{-1} that is assigned to $C{=}NH^+$ stretch.[35] They are associated with the red region in Table 2 and strongly support the existence of the intermediate X. On the other hand, the energy-minimized structure of intermediate X derived from the Gaussian calculation (Supporting Information Figure 4) closely resembles the product structures for four related compounds in the active site of OXA-24.[19] Thus, it is likely that intermediate X fits within the active site as shown in Figure 2 of Bou et al.[19] In particular, they showed that the group at the C2 position of LN-1-255, which only differs from SA-1-204 by two −OH groups in the phenyl ring, fits into the structure of the product complex without steric hindrance around the C2 position. Thus, for SA-1-204, the reaction intermediate X can be formed with little or no steric hindrance.

For the late intermediate Z (Scheme 3 and Table 3) that has also been captured by X-ray studies,[19] the peaks at 1550, 1339,

Table 3. Peak Assignment for Proposed Late Intermediate Z from Gaussian Calculations

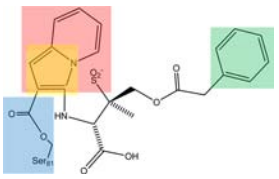

Calculation results of **late intermediate Z**			
Experimental group (cm^{-1})	Calculation group (cm^{-1})	Raman intensity (calculated)	Peak assignment
1550	1552	173	
1447	1424	62	
1339	1370	123	
1322	1355	61	
1127	1092	37	
1000	1000	30	

dx.doi.org/10.1021/ja303168n | J. Am. Chem. Soc. 2012, 134, 11206−11215

and 1322 cm^{-1} are assigned to modes of the doubly fused rings (red region). The 1447 cm^{-1} peak is assigned to the ester group, and the 1127 cm^{-1} peak is localized to the five-membered ring (yellow region). The indolizine double ring moiety gives the most intense Raman signal in the calculation of species Z, consistent with the experimental spectra. However, overall this mode is less intense than the 1658 cm^{-1} band in species X.

Because the peak at 1000 cm^{-1} is unchanged during the reaction, I_{peak}/I_{1000} can reflect the intensity change of other peaks in real time. Figure 3 plots the relative intensity of key

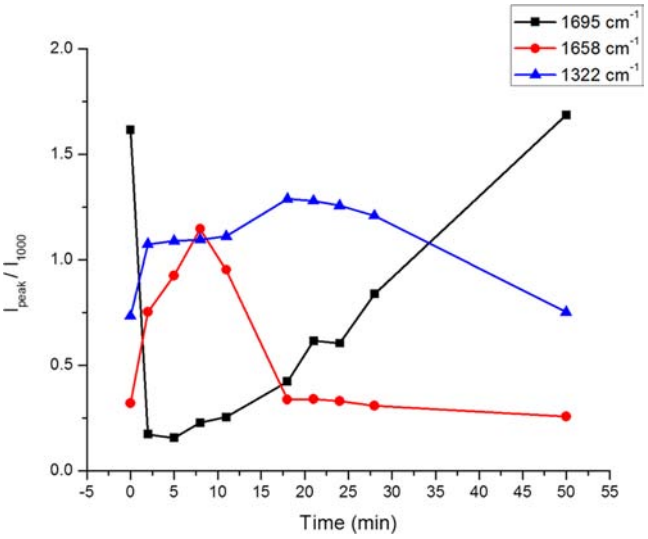

Figure 3. Kinetic depiction of the substrate peak 1695 cm^{-1}, early intermediate peak 1658 cm^{-1}, and late intermediate peak 1322 cm^{-1} intensities over time.

peaks in the Raman spectra in Figure 2B as a function of time. The intensity of the substrate peak at 1695 cm^{-1} decreases quickly as SA-1-204 is soaked in. The peak at 1658 cm^{-1} increases and decreases faster than other major peaks, indicating it originates from an early intermediate in the reaction. The late intermediate peak at 1322 cm^{-1} increases and plateaus between 2 and 18 min, then declines from 18 to 50 min, which indicates the formation of final product that leaves the active site after slowly deacylating. The substrate population declines rapidly over 2 min but then increases until at 50 min when there appears to be a stable population in the active site. A more extensive set of Raman difference spectra of OXA-24 reaction with SA-1-204 are shown in Supporting Information Figure 1, as well as a more detailed kinetic depiction of intensity changes of the main peaks (Supporting Information Figure 2). From the overall kinetic mechanism, a detailed examination reveals that the reaction follows a very clear order: substrate disappears, intermediate(s) form and leave as the product, and substrate reenters without being catalyzed.

Unexpectedly, we find that under the conditions of our reaction in the OXA-24 crystal, the reaction goes through one cycle. This finding is without precedent. Bou et al.[19] point out that in contrast to class A β-lactamase, a hydrolytic water molecule is absent in OXA-24 crystallographic structure, and, instead, the key role is played by a carboxylated Lys84;[36] this Lys84 is of central importance in OXA-24 and essential for catalytic activity.[19] In earlier work, Golemi et al.[9] also shows that at low pH, decarboxylation of the Lys70 (a structurally and mechanistically equivalent residue) leads to the inactivity of the enzyme OXA-10. When the enzyme OXA-10 is regenerated by exposure to bicarbonate, activity is restored and the degree of carboxylation correlates with the degree of recovery of activity.[37] Here, we propose that the "one cycle" of the reaction is due to the decarboxylation of Lys84 in the active site after the first reaction cycle and that in the crystal environment recarboxylation does not occur (Scheme 3). Support for a one-cycle reaction leading to an inactive enzyme is found in the solution studies described in section 3.c.

c. Recarboxylation of the Lysine Residue 84 in the Active Site Restores OXA-24's Hydrolytic Activity toward Nitrocefin in Solution. The results discussed above indicate that OXA-24 in the crystal undergoes one catalytic cycle and then becomes inactive. A possible explanation lies in the role of carboxylated lysine 84 residue in the catalytic process. All class D β-lacatamases characterized to date have a carboxylated lysine residue in the active site.[9,38−40] In OXA-10 class D β-lactamase, carboxylation is a reversible process.[9] The lysine spontaneously decarboxylates at low pH 4.5 but can be recarboxylated by exposure to 20 mM $NaHCO_3$ at pH 7.5. Golemi et al.[9] also show that the hydrolysis of most substrates by OXA-10 is characterized by biphasic kinetics due to the presence of an equilibrium between the uncarboxylated and carboxylated forms of Lys70 (see above).[37] OXA-24 class D β-lactamase also has a carboxylated Lys84 in its active site.[36] Thus, we undertook experiments in solution and in single crystals to test our hypothesis that, in the presence of SA-1-204, Lys84 in OXA-24 becomes decarboxylated during the first cycle of catalysis, rendering the enzyme inactive.

In solution, 5 μM OXA-24 was reacted with 20 μM nitrocefin. Nitrocefin was used as a chromogenic substrate to monitor the enzyme activity in solution. Almost all of the nitrocefin is transformed into product as evidenced in the 482 nm absorbance in Figure 4 (black line). Next, 5 μM OXA-24 and 50 μM SA-1-204 were mixed for 1 min, and then 20 μM nitrocefin was added. This gives rise to the absorbance peak near 380 nm in Figure 4 (red line). A nitrocefin product peak is not visible near 482 nm indicating that SA-1-204 completely blocks the activity of OXA-24 toward nitrocefin. However, when the solution of inhibited OXA-24 (with SA-1-204 and nitrocefin) is treated with 100 μM or 100 mM sodium bicarbonate ($NaHCO_3$), activity is restored and nitrocefin product appears (green and blue lines, respectively). In a control, there was no effect when 100 mM $NaHSO_4$ replaced $NaHCO_3$ (cyan line). The same experiment was also repeated in the presence of 28% PEG 2000. Not only could bicarbonate reactivate the OXA-24 enzyme but also PEG could slow both the decarboxylation and the recarboxylation process (data not shown). In addition, UV−absorbance assays show that the reaction between SA-1-204 and OXA-24 is strictly stoichiometric. While 20 μM OXA-24 and 60 μM SA-1-204 are reacted, the spectrum shows only one-third of the SA-1-204 (equivalent to the concentration of OXA-24) is hydrolyzed, indicating that the reaction undergoes only one cycle under these conditions (Supporting Information Figure 3A). Yet in the presence of $NaHCO_3$, the enzyme continues hydrolyzing SA-1-204 until the latter is exhausted (Supporting Information Figure 3B). This suggests that the enzyme becomes decarboxylated after the first reaction cycle but can be reactivated by the addition of carbon dioxide generated from bicarbonate.

To probe the reaction in a single crystal, a OXA-24 single crystal (Figure 5A) is transferred into a fresh hanging drop made up of 0.1 M HEPES (pH 7.5). The concentration of

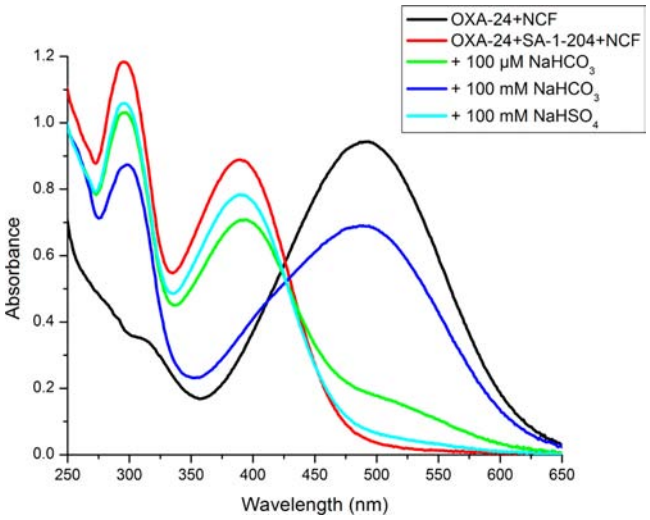

Figure 4. Recarboxylation of the lysine residue 84 in the active site can restore the OXA-24 hydrolytic activity toward nitrocefin. Black line: OXA-24 was 5 μM in HEPES buffer (10 mM, pH 7.5), then 20 μM NCF was added and the UV−absorbance spectrum was recorded. Red line: Reagents were added in the order of 5 μM OXA-24, 50 μM SA-1-204, 20 μM NCF at the intervals of 1 min, then the UV−absorbance spectrum was recorded. Green line: Reagents were added in the order of OXA-24, SA-1-204, NCF, 6 and 100 μM sodium bicarbonate, then UV−absorbance spectrum were recorded every 30 s in the next 30 min. Blue line: The same as in the green line except that the sodium bicarbonate concentration was 100 mM. Cyan line: The same as in the green line except using 100 mM sodium bisulfate.

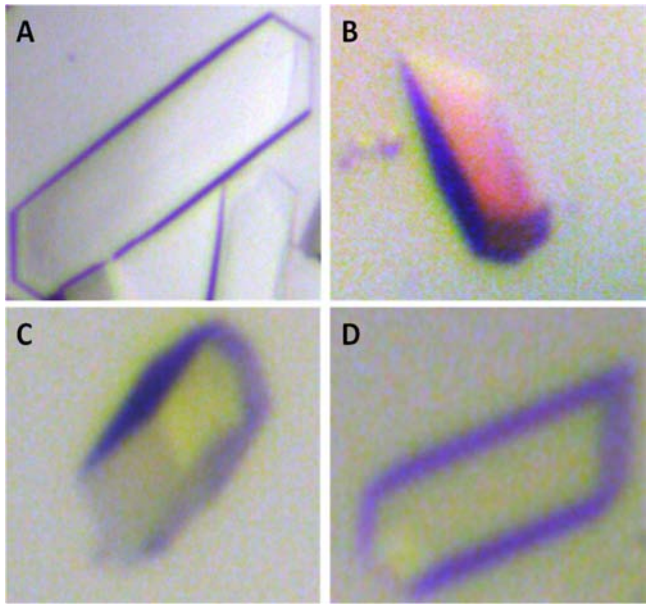

Figure 5. Low ratio of concentration between $NaHCO_3$ and OXA-24 (C_{NaHCO3}:C_{OXA-24}) is unable to reactivate the enzyme. Single OXA-24 crystal was transferred from the mother liquor solution to a 4 μL drop of 0.1 M HEPES (pH 7.5), 0.1 M NaAc, and 28% PEG 2000. SA-1-204, nitrocefin, and $NaHCO_3$ were added to test the hydrolysis activity of the crystal. (A) OXA-24 crystal in the mother liquor solution. (B) One microliter of nitrocefin (1 mg/mL) was added into the solution containing the single OXA-24 crystal. (C) One microliter of SA-1-204 (20 mM) was soaked in the single crystal solution for 1 min, then nitrocefin was added. (D) One microliter of $NaHCO_3$ (100 mM) was added into the solution after the SA-1-204 and nitrocefin mixture.

active sites is calculated as 15 mM (Supporting Information). Nitrocefin is injected into the drop to give a final concentration of 1 mM. Nitrocefin is hydrolyzed quickly within the crystal because the crystal turns red immediately (Figure 5B). When 5 mM SA-1-204 is first soaked into the drop containing a OXA-24 single crystal, no nitrocefin product is generated and the crystal remains yellow (Figure 5C). When the mixture of above OXA-24 single crystal, SA-1-204, and unreacted nitrocefin is treated with 100 mM $NaHCO_3$, nitrocefin product is still not formed and crystal does not turn red (Figure 5D), indicating that enzyme remains inactive. Thus, for the "in solution" data, the one-cycle reaction is a consequence of the lysine decarboxylation that can be rescued by the addition of $NaHCO_3$, but the activity could not be restored in single crystal. An explanation is that there is an equilibrium between the uncarboxylated and carboxylated Lys84. In the single crystal reaction, the concentration ratio between $NaHCO_3$ and decarboxylated Lys84 is about 7:1 because the protein concentration is about 15 mM (Supporting Information Text 2),[41] much lower than that in solution 1000:1, so that the Lys84 remains noncarboxylated and cannot hydrolyze the next coming nitrocefin.

Experimental evidence to date has established that the carboxylated lysine residue results from a reaction between the nonprotonated ε-amino group of the lysine and carbon dioxide.[17] Studies on OXA-10 reveal that Val117, Phe120, and Trp154 in the active site maintain a hydrophobic environment (hydrophobic pocket) for the Lys70, which decreases the pK_a of Lys70, favoring its reaction with carbon dioxide.[39,42] Crystallographic studies on the active site of OXA-24 indicate that Lys84 is also in a hydrophobic environment, which consists of Val130 and Trp167. Specifically, the residue Trp167 interacts with the carboxylate group of Lys84 and helps it locate in an "optimum orientation". This will also lead to the decrease the pK_a of Lys84, which yields a major proportion of nonprotonated ε-amino at physiological pH, favoring its carboxylation.[9,42,43] The in vivo concentration of CO_2 has been reported at 1.3 mM;[44] Golemi et al.[9] reported that the dissociation constant (K_d) for CO_2 and monomeric OXA-10 β-lactamase was 12.4 ± 0.01 μM. Considering that OXA-24 β-lactamase is also a monomer, this enzyme is expected to be fully carboxylated in its native state.

Regarding the decarboxylative mechanism, loss of CO_2 directly from the negatively charged conjugate base of the carbamic acid would involve formation of a nitrogen anion. Given the high pK_a (ca. 35) of such an unstabilized nitrogen anion, it is logical that decarboxylation of the carbamic acid occurs with concurrent transfer of a proton from oxygen to nitrogen possibly through an intermediate water molecule, predicted theoretically and shown in Scheme 2. This is consistent with the observation that decarboxylation of the lysine also occurs at pH < 4.5. Thus, for continued β-lactam hydrolysis and avoidance of decarboxylation of the carboxylated lysine, it is important for the enzyme to maintain the anionic conjugate base state of the carbamic acid moiety. In the normal hydrolytic sequence, each time the *N*-carboxy group abstracts a proton, it is rapidly removed, first ferrying a proton from the active site serine to the departing N4 as shown in Scheme 1, B to C (to assist departure of that nitrogen from the tetrahedral intermediate and prevent it from assuming a formal negative charge), and second from the hydrolytic water to the same nitrogen, this time the nitrogen acting as a simple amine base (pK_a 10−11), but nonetheless leaving the carbamic acid as its conjugate base to resume the catalytic cycle (Scheme 1, E to F).

dx.doi.org/10.1021/ja303168n | J. Am. Chem. Soc. 2012, 134, 11206−11215

With the pyridylalkylidene inhibitor, however, two events interfere with this course of events: (1) the fragmentation of the dioxothiazoline ring system, with ejection of the sulfinate anion, and concomitant intramolecular capture of the resultant imine by the pyridine nitrogen, has now created a positively charged pyridinium ion in Y (Scheme 3), which can form an aromatic indolizine system by loss of a proton from C5 (penam numbering) to the conjugate base of the carbamic acid and placing it in a (conjugate acid) state more susceptible to decarboxylation (Scheme 3, Y to Z). (2) In the subsequently formed aromatic intermediate Z, the (penam) N4 atom is now part of a β-aminoacrylate moiety, and thus has reduced pK_a (ca. 5), now insufficient to deprotonate the carbamic acid (pK_a = 6), and thus rendering the carboxylysine susceptible to decarboxylation. Once this decarboxylation occurs, the resultant amine of the lysine is too distant from the ester linkage of the acyl-enzyme to efficiently function as a base during the hydrolytic process. Even if the ester is slowly hydrolyzed, without a basic (thiazolidine) nitrogen to carry away the proton from the site, the lysine is left protonated, and unable to react with CO_2 in a carboxylative process or to function as a catalytic base to initiate acylation.

In the case of the class A β-lactamases, the hydrolytic water molecule is well ordered and observed crystallographically. By contrast, an active-site water molecule has never been observed for any class D β-lactamase.[40] Because water is required for hydrolysis of the acyl-enzyme, it is logical to propose that the hydrolytic water molecule is more disordered in class D, as they have large and more hydrophobic active sites.

Bou et al. had earlier proposed that 6-alkylidenepenicillin sulfone inhibitors, which rearrange to bulky, conformationally rigid indolizines subsequent to acylation of the active site serine, may function by displacing the hydrolytic water.[19] The present work seems to imply that, although water is displaced from a position in which it could hydrolyze the acyl-enzyme, water is still present proximal to the carboxylated lysine and is capable of facilitating its decarboxylation, as shown in Scheme 2. It is not yet clear if the water molecule that facilitates decarboxylation of the active site lysine is the same water molecule that is responsible for hydrolysis of the acyl-enzyme. Perhaps the bulky inhibitor has moved the water molecule from a position where it interacts with the terminus of the carboxylated lysine and the active site serine, to a position where it simultaneously interacts with the protonated carbamic acid and the ϵ-nitrogen of the lysine, thus facilitating decarboxylation as shown in Scheme 2.

CONCLUSIONS

In summary, the results of these experiments and the underlying mechanistic explanations provide unique insights that lead us further along the path to understanding on a very fundamental level the reaction chemistry and mechanism of inhibition of these clinically important class D OXA carbapenemases. As the pathogen harboring this β-lactamase (*A. baumannii*) has become a major threat to our antimicrobial armamentarium, new chemical approaches are desperately needed. The importance of the single turnover reaction cannot be overstated. In effect, we demonstrate that under the appropriate conditions, an OXA-24 β-lactamase is "trapped" and becomes catalytically incompetent as a result of a single turnover interaction with an inhibitor. This unprecedented observation has significant ramifications. The challenge here will be to capitalize on this finding and create novel classes of compounds that accelerate decarboxylation and retard the repopulation of Lys84 by carboxylate. This unique strategy creates an entirely new goal in synthetic chemistry that may be approached using both β-lactam scaffolds that preserve our existing drugs as well as by fragment-based libraries.[45] In the latter case, diverse chemotypes may be exploited to achieve single turnover kinetics.

ASSOCIATED CONTENT

Supporting Information

SI Figures 1−2 showing detailed Raman difference spectra of the reaction in OXA-24 crystals, kinetic trace of the main Raman peaks. SI Figure 3 showing the effect of bicarbonate on the solution reaction between OXA-24 and SA-1-204. Text showing acquisition of Raman difference spectrum and calculation of active site concentration. This material is available free of charge via the Internet at http://pubs.acs.org.

AUTHOR INFORMATION

Corresponding Author

jbuynak@mail.smu.edu; prc5@case.edu

Notes

The authors declare no competing financial interest.

ACKNOWLEDGMENTS

This work was supported by NIH GM54072 to Paul R. Carey. Robert A. Bonomo is also supported by the VISN 10 GRECC, a Merit Review Award by the VHA, and NIH RO1-AI072219-05.

REFERENCES

(1) Poirel, L.; Naas, T.; Nordmann, P. *Antimicrob. Agents Chemother.* **2010**, *54*, 24.
(2) Bou, G.; Oliver, A.; Martinez-Beltran, J. *Antimicrob. Agents Chemother.* **2000**, *44*, 1556.
(3) Poirel, L.; Marque, S.; Heritier, C.; Segonds, C.; Chabanon, G.; Nordmann, P. *Antimicrob. Agents Chemother.* **2005**, *49*, 202.
(4) Gordon, N. C.; Wareham, D. W. *Int. J. Antimicrob. Agents* **2010**, *35*, 219.
(5) Zhao, W. H.; Hu, Z. Q. *Crit. Rev. Microbiol.* **2010**, *36*, 245.
(6) Poirel, L.; Nordmann, P. *Clin. Microbiol. Infect.* **2006**, *12*, 826.
(7) Philippon, L. N.; Naas, T.; Bouthors, A. T.; Barakett, V.; Nordmann, P. *Antimicrob. Agents Chemother.* **1997**, *41*, 2188.
(8) Zavascki, A. P.; Carvalhaes, C. G.; Picao, R. C.; Gales, A. C. *Expert Rev. Anti-Infect. Ther.* **2010**, *8*, 71.
(9) Golemi, D.; Maveyraud, L.; Vakulenko, S.; Samama, J. P.; Mobashery, S. *Proc. Natl. Acad. Sci. U.S.A.* **2001**, *98*, 14280.
(10) Cha, J.; Mobashery, S. *J. Am. Chem. Soc.* **2007**, *129*, 3834.
(11) Abendroth, J.; Niefind, K.; Schomburg, D. *J. Mol. Biol.* **2002**, *320*, 143.
(12) Huang, C. Y.; Hsu, C. C.; Chen, M. C.; Yang, Y. S. *J. Biol. Inorg. Chem.* **2009**, *14*, 111.
(13) Borbulevych, O.; Kumarasiri, M.; Wilson, B.; Llarrull, L. I.; Lee, M.; Hesek, D.; Shi, Q.; Peng, J.; Baker, B. M.; Mobashery, S. *J. Biol. Chem.* **2011**, *286*, 31466.
(14) Birck, C.; Cha, J. Y.; Cross, J.; Schulze-Briese, C.; Meroueh, S. O.; Schlegel, H. B.; Mobashery, S.; Samama, J. P. *J. Am. Chem. Soc.* **2004**, *126*, 13945.
(15) Thumanu, K.; Cha, J.; Fisher, J. F.; Perrins, R.; Mobashery, S.; Wharton, C. *Proc. Natl. Acad. Sci. U.S.A.* **2006**, *103*, 10630.
(16) Llarrull, L. I.; Toth, M.; Champion, M. M.; Mobashery, S. *J. Biol. Chem.* **2011**, *286*, 38148.
(17) Li, J.; Cross, J. B.; Vreven, T.; Meroueh, S. O.; Mobashery, S.; Schlegel, H. B. *Proteins* **2005**, *61*, 246.
(18) Ruelle, P.; Kesselring, U. W.; Ho, N. T. *J. Mol. Struct. (THEOCHEM)* **1985**, *25*, 41.

(19) Bou, G.; Santillana, E.; Sheri, A.; Beceiro, A.; Sampson, J. M.; Kalp, M.; Bethel, C. R.; Distler, A. M.; Drawz, S. M.; Pagadala, S. R.; van den Akker, F.; Bonomo, R. A.; Romero, A.; Buynak, J. D. *J. Am. Chem. Soc.* **2010**, *132*, 13320.
(20) Kumarasiri, M.; Llarrull, L. I.; Borbulevych, O.; Fishovitz, J.; Lastochkin, E.; Baker, B. M.; Mobashery, S. *J. Biol. Chem.* **2012**, *287*, 8232.
(21) Wilke, M. S.; Hills, T. L.; Zhang, H. Z.; Chambers, H. F.; Strynadka, N. C. *J. Biol. Chem.* **2004**, *279*, 47278.
(22) Kalp, M.; Sheri, A.; Buynak, J. D.; Bethel, C. R.; Bonomo, R. A.; Carey, P. R. *J. Biol. Chem.* **2007**, *282*, 21588.
(23) Buynak, J. D.; Rao, A. S.; Doppalapudi, V. R.; Adam, G.; Petersen, P. J.; Nidamarthy, S. D. *Bioorg. Med. Chem. Lett.* **1999**, *9*, 1997.
(24) Altose, M. D.; Zheng, Y.; Dong, J.; Palfey, B. A.; Carey, P. R. *Proc. Natl. Acad. Sci. U.S.A.* **2001**, *98*, 3006.
(25) Dong, J.; Swift, K.; Matayoshi, E.; Nienaber, V. L.; Weitzberg, M.; Rockway, T.; Carey, P. R. *Biochemistry* **2001**, *40*, 9751.
(26) Frisch, M. J.; Trucks, G. W.; Schlegel, H. B.; Scuseria, G. E.; Robb, M. A.; Cheeseman, J. R.; Montgomery, J. A., Jr.; Vreven, T.; Kudin, K. N.; Burant, J. C.; Millam, J. M.; Iyengar, S. S.; Tomasi, J.; Barone, V.; Mennucci, B.; Cossi, M.; Scalmani, G.; Rega, N.; Petersson, G. A.; Nakatsuji, H.; Hada, M.; Ehara, M.; Toyota, K.; Fukuda, R.; Hasegawa, J.; Ishida, M.; Nakajima, T.; Honda, Y.; Kitao, O.; Nakai, H.; Klene, M.; Li, X.; Knox, J. E.; Hratchian, H. P.; Cross, J. B.; Bakken, V.; Adamo, C.; Jaramillo, J.; Gomperts, R.; Stratmann, R. E.; Yazyev, O.; Austin, A. J.; Cammi, R.; Pomelli, C.; Ochterski, J. W.; Ayala, P. Y.; Morokuma, K.; Voth, G. A.; Salvador, P.; Dannenberg, J. J.; Zakrzewski, V. G.; Dapprich, S.; Daniels, A. D.; Strain, M. C.; Farkas, O.; Malick, D. K.; Rabuck, A. D.; Raghavachari, K.; Foresman, J. B.; Ortiz, J. V.; Cui, Q.; Baboul, A. G.; Clifford, S.; Cioslowski, J.; Stefanov, B. B.; Liu, G.; Liashenko, A.; Piskorz, P.; Komaromi, I.; Martin, R. L.; Fox, D. J.; Keith, T.; Al-Laham, M. A.; Peng, C. Y.; Nanayakkara, A.; Challacombe, M.; Gill, P. M. W.; Johnson, B.; Chen, W.; Wong, M. W.; Gonzalez, C.; Pople, J. A. *Gaussian 03*, revision C.02; Gaussian, Inc.: Wallingford, CT, 2004.
(27) Shannon, K.; Phillips, I. *J. Antimicrob. Chemother.* **1980**, *6*, 617.
(28) Mei, L. H.; Lin, D. Q.; Zhu, Z. Q.; Han, Z. X. *J. Chem. Eng. Data* **1995**, *40*, 1168.
(29) Bulychev, A.; Mobashery, S. *Antimicrob. Agents Chemother.* **1999**, *43*, 1743.
(30) Helfand, M. S.; Totir, M. A.; Carey, M. P.; Hujer, A. M.; Bonomo, R. A.; Carey, P. R. *Biochemistry* **2003**, *42*, 13386.
(31) Carey, P. R. *Biochemical Applications of Raman and Resonance Raman Spectroscopies*; Academic Press: New York, 1982.
(32) Chen, Y.; Basu, R.; Gleghorn, M. L.; Murakami, K. S.; Carey, P. R. *J. Am. Chem. Soc.* **2011**, *133*, 12544.
(33) Frushour, B. G.; Koenig, J. L. *Biopolymers* **1974**, *13*, 1809.
(34) Pezolet, M.; Pigeon, M.; Menard, D.; Caille, J. P. *Biophys. J.* **1988**, *53*, 319.
(35) Kalp, M.; Totir, M. A.; Buynak, J. D.; Carey, P. R. *J. Am. Chem. Soc.* **2009**, *131*, 2338.
(36) Santillana, E.; Beceiro, A.; Bou, G.; Romero, A. *Proc. Natl. Acad. Sci. U.S.A.* **2007**, *104*, 5354.
(37) Vercheval, L.; Bauvois, C.; di Paolo, A.; Borel, F.; Ferrer, J. L.; Sauvage, E.; Matagne, A.; Frere, J. M.; Charlier, P.; Galleni, M.; Kerff, F. *Biochem. J.* **2010**, *432*, 495.
(38) Docquier, J. D.; Calderone, V.; De Luca, F.; Benvenuti, M.; Giuliani, F.; Bellucci, L.; Tafi, A.; Nordmann, P.; Botta, M.; Rossolini, G. M.; Mangani, S. *Chem. Biol.* **2009**, *16*, 540.
(39) Paetzel, M.; Danel, F.; de Castro, L.; Mosimann, S. C.; Page, M. G.; Strynadka, N. C. *Nat. Struct. Biol.* **2000**, *7*, 918.
(40) Sun, T.; Nukaga, M.; Mayama, K.; Braswell, E. H.; Knox, J. R. *Protein Sci.* **2003**, *12*, 82.
(41) Carey, P. R. *Annu. Rev. Phys. Chem.* **2006**, *57*, 527.
(42) Maveyraud, L.; Golemi, D.; Kotra, L. P.; Tranier, S.; Vakulenko, S.; Mobashery, S.; Samama, J. P. *Structure* **2000**, *8*, 1289.
(43) Santillana, E.; Beceiro, A.; Bou, G.; Romero, A. *Proc. Natl. Acad. Sci. U.S.A.* **2007**, *104*, 5354.
(44) Tien, M.; Berlett, B. S.; Levine, R. L.; Chock, P. B.; Stadtman, E. R. *Proc. Natl. Acad. Sci. U.S.A.* **1999**, *96*, 7809.
(45) Teotico, D. G.; Babaoglu, K.; Rocklin, G. J.; Ferreira, R. S.; Giannetti, A. M.; Shoichet, B. K. *Proc. Natl. Acad. Sci. U.S.A.* **2009**, *106*, 7455.